

# Therapeutic Potential of Integrated Berberine Oleate Loaded Liposomes Versus Free Berberine in Carbon Tetrachloride Induced Liver Fibrosis in Rats: A Histological and Immunohistochemical Study

**Original Article** *Walaa Omar<sup>1</sup>, Nahed I. Zohdy<sup>1</sup>, Sanaa Rady<sup>1</sup>, Manal A. Elsheikh<sup>2</sup> and Rehab A. Abdel-Moneim<sup>1</sup>*

<sup>1</sup>*Department of Histology and Cell Biology, Faculty of Medicine, Alexandria University, Alexandria, Egypt.*

<sup>2</sup>*Department of Pharmaceutics, Faculty of Pharmacy, Damanhour University, Damanhour, Egypt.*

## ABSTRACT

**Introduction:** Chronic liver diseases represent a worldwide major health problem, where fibrosis is implicated in the pathogenesis with evident impact on liver functions. Berberine (BBR) is a herbal drug that possesses a variety of pharmacological actions. However, it suffers from limited membrane permeability due to its hydrophilic nature. In this context, the current study aimed to elaborate a hydrophobic ion pair complex of berberine-oleate (BBR-OL) integrated with liposomal nanoplateform and to study its therapeutic efficacy on carbon tetrachloride (CCl<sub>4</sub>) induced liver fibrosis in adult male albino rats, in comparison with free berberine.

**Materials and Methods:** Berberine-oleate complex was prepared and loaded into liposomes. Then, its therapeutic effect was investigated in CCl<sub>4</sub> induced liver fibrosis rat model compared to free BBR. Biochemical, histological, histomorphometric, and immunohistochemical assessments of blood and liver samples were performed in different groups and followed by statistical analysis of the results.

**Results:** The proposed integrated nanoliposomes showed a nanometric size (192.2±1.07nm) and a sustained release pattern with minimum drug leakage. Histologically, rats that received BBR-OL loaded liposomes showed evident amelioration of hepatic changes and collagen deposition than those that received free BBR. Biochemically, serum level of albumin was restored to control level in BBR-OL group and the serum levels of aspartate transaminase and alanine transaminase decreased significantly in BBR-OL group in comparison to CCl<sub>4</sub> induced liver fibrosis group.

**Conclusion:** A novel integrated nano-assembly of BBR-OL loaded liposomes was successfully elaborated as a promising tool for effective treatment of liver fibrosis. The histological, immunohistochemical and biochemical evaluations have demonstrated the efficacy of BBR-OL loaded liposomes in restoring the liver structure and functions.

**Received:** 10 June 2021, **Accepted:** 24 June 2021

**Key Words:** Berberine (BBR); histological evaluation; hydrophobic ion-pair complex; liposomes; liver fibrosis.

**Corresponding Author:** Walaa Abdel Salam Ahmed Omar, MD, Department of Histology and Cell Biology, Faculty of Medicine, Alexandria University, Alexandria, Egypt., **Tel.:** +20 10 0551 7170, **E-mail:** walaaomar81@yahoo.com

**ISSN:** 1110-0559, Vol. 45, No. 3

## INTRODUCTION

Chronic liver diseases represent a major worldwide health problem with significant social and economic impact. Herein, liver fibrosis is considered an integral part in the pathogenesis of most of the chronic liver diseases, which are associated with hepatocytes degeneration, as well<sup>[1]</sup>. Furthermore, persistence of the fibrotic tissue usually ends up with cirrhosis, that is regarded as a serious health problem with risk of hepatocellular carcinoma development<sup>[2,3]</sup>. Liver fibrosis is a wound-healing procedure that occurs in response to repeated chronic liver injury from different etiologies. Hepatitis B virus (HBV) and Hepatitis C virus (HCV) infections account for the majority of the etiologies of liver fibrosis diseases worldwide. According to the world health organization

(WHO) estimation for the worldwide hepatitis infection, there are 257 million persons infected with hepatitis B worldwide with about 900000 cases of hepatitis B related mortality. Nevertheless, 71 million people are infected with hepatitis C, with about 400000 yearly related deaths<sup>[3,4]</sup>.

Throughout the literature, different strategies have been developed for treatment of liver fibrosis depending on the cause and the degree of fibrosis. Mild to moderate fibrosis can be reversible, if the causative agent is removed or treated early. As such, variable anti fibrotic drugs have been proposed to promote the resorption of excessively deposited extracellular matrix (ECM). Moreover, targeting of hepatic stellate cells (HSCs) has emerged as an equally promising complement to therapies that reduce liver injury, where it is suggested to have a key role in pathogenesis

of fibrosis<sup>[5-7]</sup>. However, liver transplantation is so far the principal treatment modality for advanced liver fibrosis, yet it has not been validated to be positive in the long-term due to the limited availability of the donors, long waiting lists, its high cost and the possibility of organ rejection<sup>[8]</sup>.

Recently, herbal medicines have demonstrated promising therapeutic potential in liver fibrosis treatment through various mechanisms of action<sup>[9]</sup>. Berberine (BBR) is an isoquinoline alkaloid that is isolated from a range of Chinese herbs, and was used in the Chinese medicine in the treatment of many gastrointestinal diseases. It has been ascribed many pharmacological actions including; anti-microbial, anti-inflammatory, anti-oxidative and anti-tumor activities<sup>[10-13]</sup>. Previous research work has demonstrated the potent role of BBR in treatment of liver fibrosis<sup>[14,15]</sup>. However, BBR is a hydrophilic compound with limited permeability and bioavailability, which hinder its therapeutic efficacy in clinical practice. Thus, throughout the literature, different approaches of drug development aimed to improve the drug bioavailability through changing its physicochemical properties and hence improve the solubility and bioavailability, such as size reduction, solid dispersion, use of surfactants, phospholipid complexation, and others<sup>[16-20]</sup>.

Although, the hydrophobic ion-pairing tactic is reported to be an efficient strategy, which promotes the formation of hydrophobic BBR analogue with improved absorption through lipophilic membranes, biodistribution and bioavailability, yet a more optimum nanocarrier drug delivery system has been proposed<sup>[21-25]</sup>.

Recently, nanocarriers have emerged as a promising approach for drug delivery, where loading drugs on carriers ranging in size from 10-500 nm improves the physicochemical properties of the drug, membrane permeability, targetability and hence the therapeutic efficacy. Moreover, it minimizes the possible undesirable effects of drugs<sup>[26-30]</sup>. Liposomes are small spherical vesicles that range from 30 nm to several micrometers. They consist of one or more lipid bilayers surrounding aqueous units, where the polar heads are oriented externally and internally towards the aqueous medium, thus mimicking the cell membrane. Besides the advantage of biocompatibility, biodegradability and low toxicity profile, liposomes afford versatility in loading either hydrophilic or hydrophobic compounds. Therefore, they are regarded as the most promising platforms as drug carriers for enhancing therapeutic efficacy of many drugs<sup>[31]</sup>. However, one of the liposomes' drawbacks is the quick drug release. Recently, a novel "hybrid nano-assemble" approach was developed to minimize such leakage from the liposomes<sup>[32-34]</sup>. In this context, the current study aimed to utilize the benefits of hydrophobic ion paired approach along with liposomes to fabricate a novel integrated nano-assembled liposomal nanocarrier loaded with berberine-oleate (BBR-OL) complex for efficient management of an experimentally induced liver fibrosis rat model, in comparison with free berberine.

## MATERIALS AND METHODS

### Materials

Carbon tetrachloride (99.5% purity) was purchased from Chema tech Co. (Tianjin, China). Soybean phosphatidylcholine (molecular weight=766) was purchased from Lipoid AG (Ludwigshafen, Germany). Cholesterol was a kind gift from The Nile for Pharmaceuticals and Chemical Industries (Cairo, Egypt). Berberine hydrochloride was purchased from Baoji Guokang Bio-Technology Co, Ltd China. Sodium oleate was purchased from Sigma-Aldrich (St. Louis, MO, USA). All the other chemicals, solvents and reagents were of analytical grade.

### Animals

Forty adult male albino rats (6-8 weeks old, 150-200 g) were housed under standard laboratory conditions of temperature and humidity and 12 h light/dark cycle. They were fed standard laboratory diet and tap water. The animal studies were performed after receiving approval of the institutional review board of ethics, Faculty of medicine, University of Alexandria IRB NO:00012098).

### Preparation of liposomes

#### Preparation of berberine-oleate complex

The berberine-oleate (BBR-OL) complex was prepared by hydrophobic ion-pairing technique as mentioned previously by Torky *et al.*<sup>[24]</sup>. Briefly, sodium oleate (SO) aqueous solution (100mg/ml) was added drop wise onto BBR aqueous solution (1 mg/ml) at molar ratio of (1:1) under magnetic stirring at 400 r.p.m. and room temperature. The precipitate left was separated by centrifugation at 15,000 r.p.m. for 30 min and then collected as BBR-OL complex for further testing.

#### Characterization of berberine-oleate complex

##### Determination of complexation efficiency (CE%)

The complexation efficiency between BBR and SO with 1:1 stoichiometry was determined as reported by Torky *et al.*<sup>[24]</sup>. The concentration of residual un-complexed BBR in the supernatant after centrifugation was quantified using spectrophotometer at  $\lambda_{max}$  346 nm. Then (%CE) was calculated according to the following equation (Eq.1):

$$\%CE = \frac{\text{(The total amount of the added BBR-BBR's amount in supernatant)}}{\text{The total amount of the added BBR}} \times 100 \dots \text{Eq.1}^{[27]}$$

#### Fourier transform infrared spectroscopy (FTIR)

Different samples (BBR, SO and BBR-OL complex) were triturated separately with dry crystalline potassium bromide to a fine powder and compressed into disc under a hydraulic press at 10,000 psi for 30 seconds. Each potassium bromide disc was scanned within a wave number region of 4000–500/cm-1 using a Fourier transform infrared (FTIR) spectrometer (PerkinElmer Inc, NY, USA)<sup>[24]</sup>.

### **X-Ray Diffraction (XRD)**

The X-ray diffraction of BBR, SO and BBR-OL complex was carried out using XRD-7000 diffractometer. The diffraction pattern was carried out with a voltage of 30 kV and a current of 30 mA and the spectra of graphs were plotted within the range of  $2\theta$  ( $10^\circ$ -  $40^\circ$ ) with continuous scanning<sup>[35]</sup>.

### **Preparation of empty and berberine loaded-liposomes**

Ethanol injection method was used for the preparation of liposomes. Briefly, lipid mixture of Lipoid S100 (L- $\alpha$ -phosphatidylcholine) and cholesterol was dissolved in 2 ml absolute ethanol at weight ratio of 5:1 respectively. Then, the resulting ethanolic solution was injected, drop wise through syringe of gauge size = 23, into 10 ml deionized water under magnetic stirrer at 800rpm at room temperature and left for an hour on the stirrer. Finally, liposomal suspensions were kept overnight in refrigerator for stabilization before further characterization. For BBR-OL complex loading in liposomes, a quantity of BBR-OL complex (equivalent to 30 mg BBR) was dissolved in the ethanolic solution of lipids<sup>[36]</sup>. Then, the next steps were carried out as mentioned previously in the preparation of liposomes.

### **Characterization of empty and berberine loaded liposomes**

#### **Particle size, polydispersity index and $\zeta$ -potential**

The mean particle size,  $\zeta$ -potential ( $Z_p$ ) and polydispersity index (PDI) of the prepared liposomes were determined by dynamic light scattering technique using Malvern Zetasizer (Malvern Instruments Ltd., Malvern, UK). The samples were diluted 10- to 20-folds with filtered distilled water and put in ultrasound bath sonicator for 5min prior to measurements at  $25^\circ\text{C}$  and at an angle of  $173^\circ$ . Measurements were done in triplicate and the value recorded is the mean  $\pm$ SD<sup>[33]</sup>.

#### **Transmission electron microscopy**

Liposomes were identified morphologically using transmission electron microscopy (TEM; JEM-100 CX Electron Microscope, JEOL, Tokyo, Japan). Aqueous dispersion of freshly prepared samples was diluted with filtered de-ionized water (1:10) and sonicated for 5 min. Then, a drop of the dispersion was placed on a copper grid and excess suspension was removed by filter paper followed by air- drying before imaging. Samples were subsequently stained with a saturated solution of uranyl acetate for 30 seconds<sup>[37]</sup>.

#### **Measurement of Entrapment efficiency (EE%)**

Dialysis bag method was used to separate free untrapped drug from liposomes as reported by Freag M S<sup>[34]</sup>. Briefly, 0.5 ml of the drug-loaded liposomes was placed in a dialysis bag (15 kD, Sigma, MO, USA) and dialyzed against water (50 ml; achieving sink conditions)

at 500 r.p.m. for 30 min. The dialysate-containing free drug was then diluted with water and analyzed spectrophotometrically at  $\lambda_{\text{max}}$  346. The difference between the total amount of BBR used initially in preparation of liposomes and the amount of free BBR was considered as the actual drug amount encapsulated in the liposomes. (Eq.2)

$$\%EE = \frac{\text{(Actual amount of BBR entrapped in Liposomes)}}{\text{(The total amount of the added BBR)}} \times 100 \text{..Eq.2}^{[34]}$$

### **Drug release study**

Dialysis bag diffusion technique was used to investigate the release behavior of both free BBR and BBR-OL-Liposomes formulation using a dialysis membrane with a molecular weight of 12,000–14,000 Da. Samples of 1 ml of free BBR and BBR-OL-Liposomes (equivalent to 1.5 mg BBR) were placed in a dialysis bag of 5 cm length and immersed in a beaker containing 50 ml of the release medium, phosphate-buffered saline (PBS) with pH adjusted at 6.8. The beakers were kept in shaking water bath at  $37^\circ\text{C}$  with a shaking rate of 100 r.p.m. At time intervals (0.15, 0.5, 1, 2, 3, 6, 16 and 24 h), 3 ml sample of the release medium was withdrawn then compensated with the same volume of fresh release medium. The samples were then measured spectrophotometrically at  $\lambda_{\text{max}}$  346 nm using the corresponding fresh release medium as a blank<sup>[36]</sup>.

### **Animal studies**

#### **Induction of fibrosis**

24 rats received intra peritoneal (IP) injection of CCl<sub>4</sub> diluted 1:1 in olive oil at a dose of 1 ml/kg body weight twice a week for 10 weeks. At the end of the 10<sup>th</sup> week, seven rats died. The dead rats were replaced by other rats to preserve the total number of animals enrolled in the experiment and were given CCl<sub>4</sub> similarly. Liver fibrosis rat model was achieved using (IP) injection of CCl<sub>4</sub> diluted 1:1 in olive oil at a dose of 1 ml/kg body weight twice a week for 10 weeks<sup>[38,39]</sup>.

#### **Experimental design**

Forty rats were divided into four main groups as follows; Control Group (CG), Liver Fibrosis Group (LFG), Withdrawal Group (WG) and Treatment Group (TG).

Control Group (CG) (n=16 rats) Rats were equally subdivided into four subgroups;

**CGI**; received daily IV injection of 1 ml/kg distilled water (the vehicle for BBR), in the tail vein, for 6 weeks.

**CGII**; received IP injection of 1 ml/kg body weight olive oil (the vehicle for CCl<sub>4</sub>) twice weekly for 10 weeks.

**CGIII**; received daily IV injection of 10 mg/kg body weight BBR dissolved in distilled water, in the tail vein, for 6 weeks<sup>[40]</sup>.

**CGIV**; received daily IV injection of 10 mg/kg body weight BBR-OL loaded on nano-liposomes, in the tail vein, for 6 weeks<sup>[36,40]</sup>.

At the end of ten weeks, the 24 rats that received CCl<sub>4</sub> were randomly allocated into the following groups:

Liver Fibrosis Group (LFG) (n=6 rats) Rats received IP injection of CCl<sub>4</sub> diluted 1:1 in olive oil at a dose of 1 ml/kg body weight twice a week for 10 weeks only.

Withdrawal Group (WG) (n=6 rats) received no further CCl<sub>4</sub> after the ten weeks duration and were left without any treatment for additional six weeks.

Treatment Group (TG) (n=12 rats) were randomly and equally subdivided into two subgroups and the experimental duration extended for another six weeks.

Berberine Group (BG); received a daily IV dose of 10 mg/kg body weight of free berberine dissolved in distilled water<sup>[40]</sup>.

Berberine-oleate Loaded Liposomes Group (BLG); received a daily IV dose of 10 mg/kg body weight of berberine-oleate liposomes dissolved in distilled water<sup>[36,40]</sup>.

### Biochemical Assessment

Blood samples were collected from the retro-orbital plexus before scarification of animals in plain tubes and left for 30 min to clot. The serum was isolated within 1 h by centrifugation at 2000g for 10 min. Sera from all groups were stored at -80 °C. Automated Chemical Analyzer (7600; Hitachi, Tokyo, Japan) was used to measure the serum enzymes aspartate transaminase (AST) and alanine transaminase (ALT) and albumin according to the manufacturers' instructions<sup>[41]</sup>.

### Histological Study

Animals of different experimental groups were sacrificed after the decided duration for each group, and the liver was excised, and then cut into two parts. The first part was fixed in 10% formol saline and processed to get 5 µm thick paraffin sections. Some of these sections were stained with Hematoxylin and Eosin (H & E) stain and others with Masson's trichrome stain for light microscopic (LM) examination. These sections were examined with an Olympus light microscope (LM) (Olympus BX41, Tokyo, Japan) equipped with spot digital camera (Olympus DP20) at the center of excellence, CERRMA, Faculty of Medicine, University of Alexandria, Egypt<sup>[42]</sup>.

The liver fibrosis was assessed and graded according to the scoring system of Ishak *et al.*<sup>[43]</sup> where 0 = no fibrosis, 1 = expansion of some portal areas with/without septa, 2 = expansion of most portal areas with/without septa, 3 = expansion of most portal areas with portal-portal bridging, 4 = expansion of most portal areas with portal-portal and portal-central bridging, 5 = bridging with occasional nodules, 6 = cirrhosis probable or definite.

The second part of liver specimens was cut into small pieces (0.5- 1 mm<sup>3</sup>) and immediately fixed in 3% phosphate-buffered glutaraldehyde. Then tissue samples were processed into ultrathin sections, mounted on copper grids and examined and photographed by TEM (JEM-100 CX Electron Microscope, JEOL, Tokyo, Japan) at the Electron Microscope Unit in the Faculty of Science, Alexandria University, Egypt<sup>[44]</sup>.

### Immunohistochemical Study using anti alpha smooth muscle actin

Positively charged slides were used for mounting the 5µ thick liver tissue sections obtained from paraffin blocks of formol saline fixed tissue specimens. The adopted technique in the immune staining followed the streptavidin–biotin-immunological detection of alpha smooth muscle actin (α-SMA) protocol as mentioned in the manufacturer's protocol. The primary antibodies anti-smooth muscle actin (Mouse monoclonal antibody, Thermo, diluted at 1:800) as well as the detection system kit (UltraVision detection system, ThermoScientific, Fremont, CA, USA) were purchased from Lab Vision Corporation (Thermo Fisher, Fremont, USA). Positive and negative controls were used as guide in all reactions. Finally, slides were counter-stained with hematoxylin<sup>[45]</sup>.

### Histomorphometric Study

Digital images were obtained from the immunohistochemically and Masson's trichrome stained sections, using a digital camera (Olympus DP20) connected to the microscope (Olympus BX41) at magnification of 100. Six randomly selected sections from each group were subjected to histomorphometric study using NIH Fiji© program (NIH, USA). Measurements were expressed in the form of a percentage area of positive reaction to anti α-SMA or bluish green collagen trichrome stained areas. Data were presented as mean ±Standard Deviation (SD) (n=6/group)<sup>[46]</sup>.

### Statistical Study

All serological and morphometric results were analyzed using IBM SPSS software package version 20.0. (Armonk, NY: IBM Corp). Kolmogorov-Smirnov test was used to verify the normality of distribution. Quantitative data were expressed as mean ± SD. ANOVA was used for normally distributed quantitative variables, to compare between more than two groups, Post Hoc test (Tukey), and were considered significant when  $P \leq 0.05$ <sup>[47]</sup>.

## RESULTS

### Preparation and Characterization of BBR-OL complex

#### Determination of complexation efficiency (CE%)

The extent of ion pairing was determined by measuring residual un-complexed BBR in the aqueous supernatant spectrophotometrically at  $\lambda_{max}$  346. The results of

complexation efficiency were calculated and found to be  $83.53 \pm 2.41$  % which came in a good agreement with the previously reported data<sup>[24]</sup>.

#### **Fourier transform infrared spectroscopy (FTIR)**

The possible chemical interaction between BBR and SO was investigated by simple FTIR study (Figure 1). The FTIR spectrum of BBR revealed the existence of peak at 2844  $\text{cm}^{-1}$  corresponding to the methoxyl group, and the peak of the iminium ( $\text{C}=\text{N}^+$ ) double bond at 1635  $\text{cm}^{-1}$ . Whereas, the absorption signals corresponding to 1569 and 1505  $\text{cm}^{-1}$  represent the aromatic  $\text{C}=\text{C}$  bending and the furyl group, respectively. Regarding, FTIR spectrum of sodium oleate (SO), it revealed peak at 1682.4  $\text{cm}^{-1}$  due to the ( $-\text{COO}-$ ) symmetric stretching and another absorption signal at 1448.2  $\text{cm}^{-1}$  corresponding to ( $-\text{CH}_2-$ ) bending vibration. On the other hand, the FTIR spectrum of BBR-OL complex revealed a disappearance of the characteristic carboxylic group stretching band of SO at 1564.0  $\text{cm}^{-1}$  and iminium ( $\text{C}=\text{N}^+$ ) double bond peak of BBR at 1635  $\text{cm}^{-1}$ . These finding revealed the occurrence of ionic interaction between the carboxyl group of the anionic sodium oleate with the iminium ( $\text{C}=\text{N}^+$ ) group of BBR molecule. In addition, the absorption signals corresponding to  $-\text{CH}$  stretching vibration at 2938.1 and 2864.3  $\text{cm}^{-1}$  were observed<sup>[24]</sup>.

#### **X-ray powder diffraction (XRD)**

The X-ray diffractograms of BBR, SO and BBR-OL complex were depicted in (Figure 2) and came in accordance with that reported by Torkey *et al.*<sup>[24]</sup>. Diffractogram of BBR showed intense peaks at  $2\theta$  of 18.5°, 24.53°, 25.96° confirming its crystalline nature. The XRD pattern of SO demonstrated intense peaks at  $2\theta$  of 20.55° and 30.52°, reflecting its crystalline nature. Finally, XRD of the formed BBR-OL complex demonstrated intense peaks at  $2\theta$  of 15.6°, 19.8°, 25.1° and 28.2°. Therefore, these investigations demonstrated the formation of new crystalline complex between BBR and sodium oleate.

#### **Characterization of empty and BBR-OL loaded liposomes**

##### **Droplet size, PDI, $\zeta$ -potential and EE%**

Liposomes under investigation were prepared by ethanol injection method<sup>[33,48]</sup>. Such method possesses the privileges of being simple, giving homogenous size distribution with higher encapsulation efficiency and smaller vesicle sizes<sup>[48,49]</sup>. (Table 1) showed a particle size of empty liposomes of (138.9 $\pm$ 0.43nm) which increase to (192.2 $\pm$ 1.07nm) upon loading with BBR-OL complex with high EE% (78.39 $\pm$  5.09%). On the other hand, the PDI is a measure of the uniformity of particle diameter and can be used to depict the size distribution homogeneity. PDI varies from 0.0 to 1.0. The closer to zero the polydispersity value, the more homogeneous the particles are<sup>[49]</sup>. Our results demonstrated the formation of homogenous empty and drug-loaded liposomal preparations with PDI values

of (0.345 $\pm$ 4.6 and 0.149 $\pm$ 13, respectively). Concerning the zeta potential measurement, it is considered an indicator for the charge of the droplets and hence the physical stability of the colloidal system<sup>[49]</sup>. In the current investigation,  $\zeta_p$  of BBR-OL complex-loaded in liposomes demonstrated higher negative value (-23.2 $\pm$ 3.64 mV) versus the empty liposomes (-12.6 $\pm$ 4.96 mV) owing to the introduction of negative SO moiety.

#### **Transmission Electron Microscope**

As shown in (Figure 3), TEM confirmed the typical vesicular structure of both the empty and the BBR-OL loaded liposomes. Empty liposomes showed obvious hollow bright core vesicles that were surrounded by a bilayer membrane shell. On the other hand, the BBR-OL loaded liposomes appeared as electron dense vesicles. The size of the vesicles was within the same range measured using the Zetasizer; empty liposomes size range (138.9 $\pm$ 0.43nm) and BBR-OL loaded liposomes range (192.2 $\pm$ 1.07nm).

#### **Drug release studies**

It was reported that, the release profile of hydrophobic ion pair complex from nanocarriers differs according to the type of delivery vehicle used. As long as the drug is in ion pair complex it will act like a hydrophobic molecule<sup>[50]</sup>. In the current investigation, the release patterns of free BBR and BBR-OL liposomes were assessed in PBS release medium (pH 6.8) using dialysis tubing (12000–14000 Da). As shown in Figure 4, free BBR solution was mostly diffused (95.93 $\pm$ 0.98%) from the dialysis bag into the medium in the first 30 min till completely diffused in 1h. On the other hand, loading BBR-OL complex into liposomes implied an initial slow release, since; only 15.98 $\pm$ 1.11% of BBR was diffused from BBR-OL liposomes after 30 min. Then, the release from BBR-OL liposomes had reached a plateau at about 60% release after 3h and continued up to 24h with no significant change (Figure 4).

#### **Animal studies results**

##### **Biochemical Results**

In the current work, and as shown in (Figure 5a), following CCl<sub>4</sub> administration for 10 weeks, the mean levels of ALT and AST were significantly increased in the LFG and WG as compared to the CG ( $p \leq 0.001$ ). Meanwhile, both BG & BLG depicted reduced levels of ALT and AST in comparison to LFG, whereas BLG demonstrated reduced levels of ALT and AST significantly as compared to LFG.

As for serum albumin levels, and as shown in (Figure 5 b,a) significant decrease was demonstrated in both the LFG and the WG ( $p \leq 0.001$ ) as compared to the CG. Whereas, serum albumin level was increased in both BG & BLG and was recovered to the control level in BLG.

## **Histological and Histomorphometric Results**

### **Light Microscopic Results, H & E stain**

Control group (CGI, CGII, CGIII and CGIV): Classical hepatic architecture was observed with hepatocytes arranged in cords radiating from the central veins (CV). Hepatocytes appeared polyhedral with acidophilic granular cytoplasm and central rounded vesicular nuclei, and some cells appeared bi-nucleated. Hepatic sinusoids were observed as narrow spaces in between the hepatic cords lined by flat endothelial cells and few bulging Kupffer cells. The portal tracts (PT) were seen at the periphery of the hepatic lobules and are formed of a branch of the hepatic artery, a branch of the portal vein and a bile duct. The liver fibrosis stage according to Ishak was 0. (Figure 6 a,b)

Liver Fibrosis Group (LFG): Examination of Liver sections of the LFG revealed evident distortion of the hepatic architecture. Prominent connective tissue (CT) septa were noticed connecting adjacent portal areas with the formation of pseudo lobules. Hepatocytes depicted variable degenerative changes, more pronounced in the centrilobular area, in the form of hyper-eosinophilic cytoplasm with loss of granularity and indistinct cellular boundaries. Some other hepatocytes appeared pale, swollen with cytoplasmic vacuolization and an eccentric nucleus. Regarding the nuclear changes, some nuclei appeared dark shrunken, some other nuclei exhibited abnormal chromatin pattern (karyolysis) and others appeared with margination of the nucleolus. In addition, marked mononuclear cellular infiltration was evident mainly in the portal areas and in-between the hepatocytes. Dilated blood sinusoids were observed together with prominent nuclei of Kupffer cells along their lining. The portal areas appeared with congested blood vessels and proliferation of bile ducts. The liver fibrosis stage according to Ishak was 3. (Figure 6 c-f)

Withdrawal group (WG): Examination of liver sections from the WG, revealed almost the same histological features as the LFG. The liver fibrosis stage according to Ishak was 3. (Figure 7 a-c)

Treatment Group (TG) that included two subgroups; Berberine Group (BG): Partial amelioration of the degenerative changes was noticed as compared to LFG. Connective tissue septa and pseudo-lobulation were less evident. Some hepatocytes appeared polyhedral in shape with granular acidophilic cytoplasm and rounded vesicular and central nuclei, while some others exhibited hyper eosinophilic homogenous cytoplasm and dark shrunken nucleus. Some portal areas appeared with congestion of their portal vein branchess. In addition, limited periportal mononuclear cellular infiltration was still focally observed. Dilated sinusoids were noticed in some areas. The liver fibrosis stage according to Ishak was 2. (Figure 7 d-f)

Berberine-Oleate Liposomes Group (BLG): Remarkable restoration of the classical histological features

of the liver was observed. Most of the CT septa disappeared and the general architecture was restored nearly back to normal. Hepatocytes appeared large, polyhedral, with a granular acidophilic cytoplasm and large central vesicular nuclei; many were binucleated. Few hepatocytes appeared vacuolated with a signet ring appearance. Minimal periportal cellular infiltration was rarely encountered. The liver fibrosis stage according to Ishak was 1. (Figure 7 g-i)

### **Light Microscopic Results, Masson's Trichrome stain**

The trichrome stained sections of the CG showed normal pattern of collagen fibers' distribution, where minimal green trichrome stained areas were seen, surrounding the central veins and the portal areas. Rats of the LFG and the WG, showed markedly increased green trichrome stained areas, around central veins, portal areas and in the perisinusoidal spaces, forming septa and pseudo-lobules. A remarkable decrease in the green trichrome stained areas was noticed in the BG, where the septa disappeared. Whereas BLG exhibited limited green trichrome stained areas around the central veins and in the portal areas, almost mimicking the CG pattern. (Figure 8 a-e)

### **Histomorphometric Results**

The results of the trichrome stained sections that assess collagen distribution were supported by the morphometric studies as shown in (Figure 8 f), where the area percentage % of collagen was compared in the different groups. It was found that, the LFG and WG showed significant increase in collagen deposition as compared to the CG ( $P \leq 0.001$ ). The BG & BLG showed a decrease in the collagen deposition as compared to the LFG. However, the BLG showed significant decrease.

### **Transmission Electron Microscope Results**

Control groups (CGI, CGII, CGIII and CGIV): Hepatocytes were observed with their classical polyhedral shape, distinct cell boundaries together with euchromatic nuclei. Most of the mitochondria (M) appeared normal in shape. Regular profiles of rough endoplasmic reticulum (rER) were frequently encountered. Normal distribution of glycogen granules was also noticed. (Figure 9 a)

Liver Fibrosis Group (LFG): Some hepatocytes depicted shrunken nuclei with irregular outline. Most of the mitochondria appeared distorted with indistinct cristae. Dilated profiles of smooth endoplasmic reticulum (sER) together with irregular few dilated rER cisternae were observed. Moreover, glycogen granules were not abundantly distributed within the cytoplasm. Evident deposition of collagen fibrils was seen within the perisinusoidal spaces. (Figure 9 b-d)

Withdrawal group (WG): The ultra-structural results of liver sections of this group showed very close similarity to those of the fibrotic group. (Figure 10 a,b)

**Berberine Group (BG):** Partial amelioration of degenerative changes was observed in liver sections of this group, where some hepatocytes appeared with distinct cell boundaries and euchromatic nuclei. As regards the mitochondria, some appeared with distinct cristae and regular shapes, while others were still distorted with increased electron density. Few regular profiles of rER were also observed. Some dilated profiles of sER were still observed. (Figure 10 c,d)

**Berberine Oleate Loaded Liposomes Group (BLG):** Remarkable restoration of the classical ultra-structural features of hepatocytes was observed, where most of hepatocytes appeared with distinct cell boundaries and nuclei with normal chromatin pattern. Most of the mitochondria were observed with distinct cristae and regular shapes. Regular profiles of rER were frequently encountered together with apparently normal pattern of sER profiles. Glycogen granules were abundantly observed. (Figure 10 e,f)

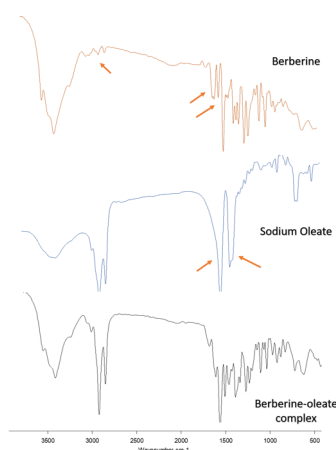


**Fig. 1:** Infrared spectroscopy of berberine, sodium oleate and berberine-oleate complex

### Immunohistochemical Results

The anti  $\alpha$ -SMA stained sections of the CG showed normal pattern of  $\alpha$ -SMA distribution within cytoplasm of smooth muscle cells in the wall of CV & PT blood vessels, in the form of brown stained areas. Rats of the LFG and the WG, showed markedly increased anti  $\alpha$ -SMA stained areas, and were seen extending in between hepatocytes, within the connective tissue septa. A decrease in the anti  $\alpha$ -SMA stained areas was noticed in the BG as compared to LFG & WG, whereas, in BLG, the normal distribution of  $\alpha$ -SMA was seen around the CVs and PTs, nearly similar to the CG pattern. (Figure 11 a-e)

The results of the anti  $\alpha$ -SMA stained sections were supported by the morphometric studies as shown in (Figure 11 f), where the area percentage % of positive reaction to anti  $\alpha$ -SMA was compared in the different groups. It was found that, the LFG and WG showed significant increase as compared to the CG ( $P \leq 0.001$ ). On the other hand, the BG and the BLG showed decreased reaction compared to LFG with a significant decrease demonstrated in BLG ( $P \leq 0.05$ ).

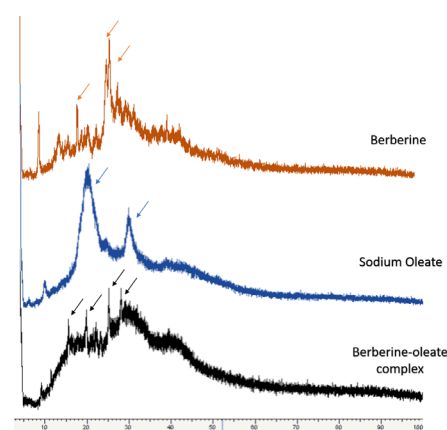


**Fig. 2:** X-ray diffraction of berberine, sodium oleate and berberine-oleate complex

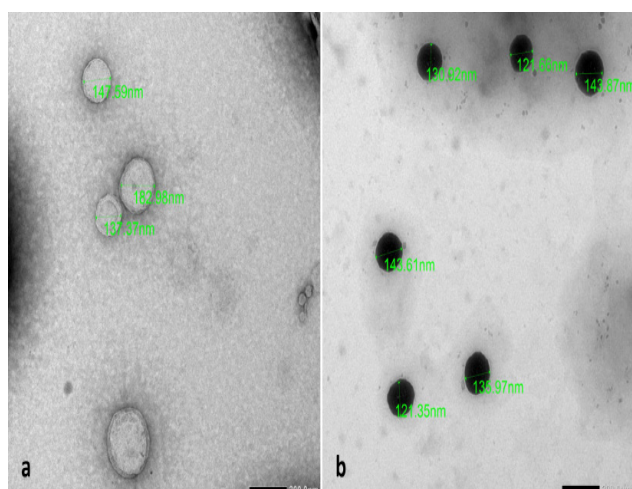


**Fig. 3:** Transmission electron micrographs of (a) empty liposomes vesicles with an obvious core and shell structure and (b) berberine-oleate loaded liposomes with dense core Microscopic (Mic) magnification (Mag) x 20,000.

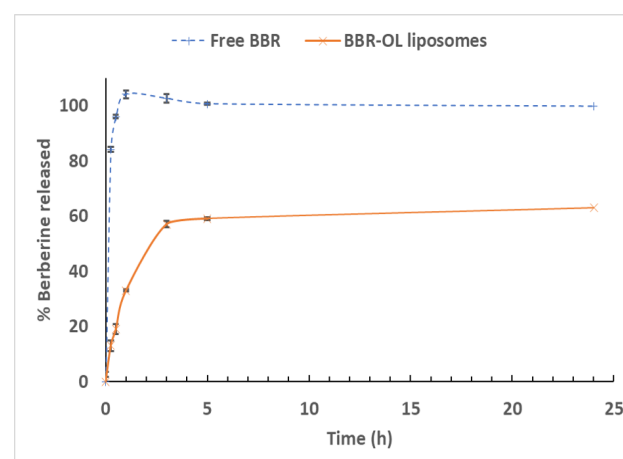


**Fig. 4:** *In vitro* release study of free BBR and BBR-OL liposomes in PBS pH 6.8 at 100 r.p.m. and 32°C using dialysis bag method. Data are expressed as a mean  $\pm$  SD (n = 3)

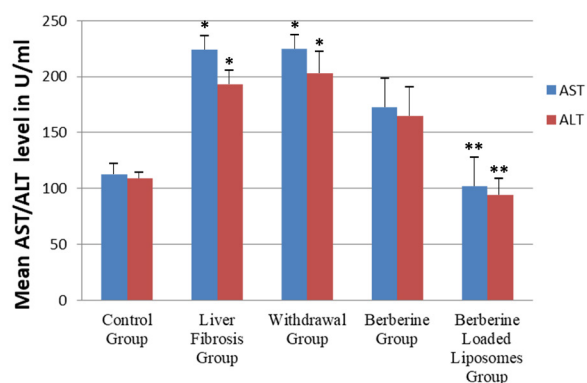


**Fig. 5a:** Serum AST & ALT levels (U/ml). Values represent mean  $\pm$  SD (n=6). Statistical significance was determined using ANOVA test. Pairwise comparison between each 2 groups was done using Post Hoc Test (Tukey) and was considered significant when  $P \leq 0.05$ . \* Indicates significant statistical difference compared to the CG. \*\* Indicates significant statistical difference compared to the LFG. It reveals that the CCl<sub>4</sub> treatment led to significant increase in mean levels of AST & ALT in LFFG and WG in comparison to control group. These levels are significantly decreased in the BLG compared to the LFG.

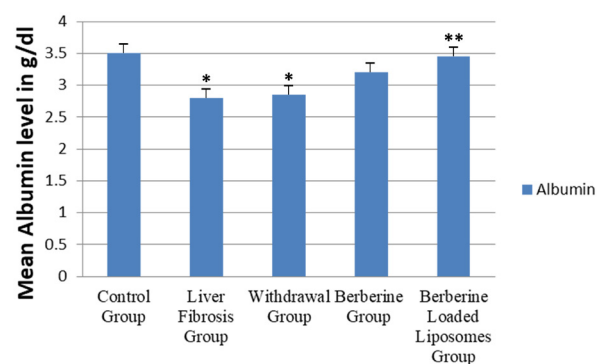


**Fig. 5b:** Serum Albumin levels (g/dL). Values represent mean  $\pm$  SD (n=6). Statistical significance was determined using ANOVA test. Pairwise comparison between each 2 groups was done using Post Hoc Test (Tukey) and was considered significant when  $P \leq 0.05$ . \* Indicates significant statistical difference compared to the CG. \*\* Indicates significant statistical difference compared to the LFG. It reveals that the CCl<sub>4</sub> treatment led to significant decrease in mean levels of serum albumin in both LFG and WG in comparison to control CG. These levels are significantly increased in the BLG compared to the LFG.

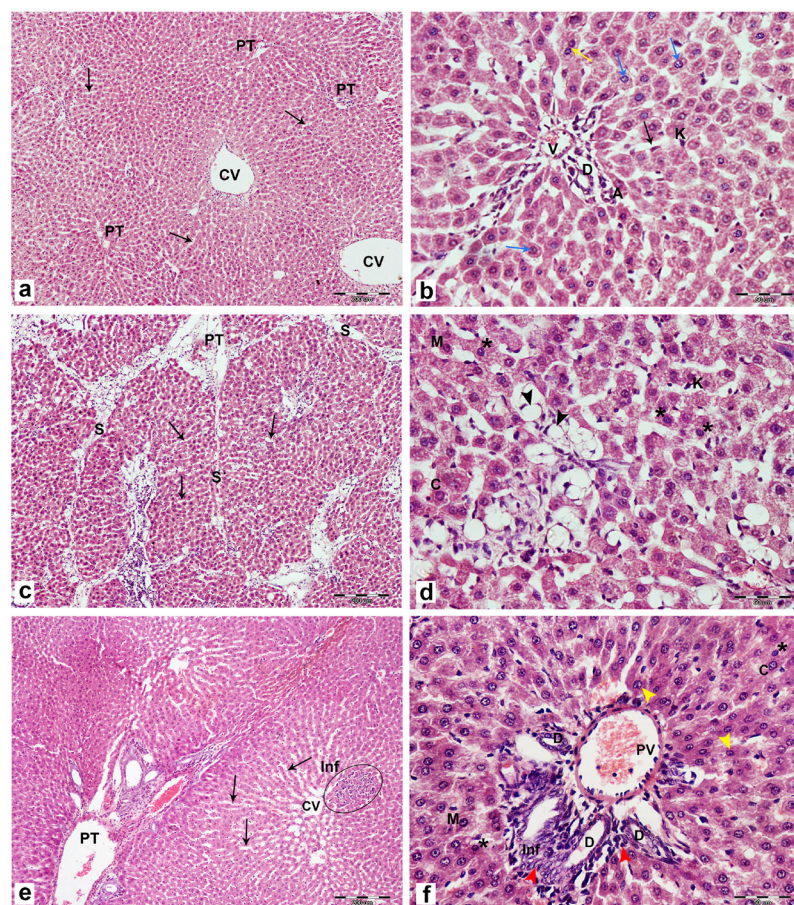


**Fig. 6:** Representative LM photographs of H & E stained liver sections (a & b) CG. (a); Cords of hepatocytes radiating from the central vein (CV) & separated by blood sinusoids (thin black arrows). Portal tracts (PT) are well defined at the angles of the hepatic lobules. (b); Hepatocytes (blue arrow) appear arranged in cords, polyhedral with acidophilic, granular cytoplasm & central vesicular nuclei. Some hepatocytes are binucleated (yellow arrow). Blood sinusoids are seen lined by endothelial cells (thin arrow) and Kupffer cells (K). The portal tract is seen containing a branch of hepatic artery (A), branch of portal vein (V) & bile duct (D). (c - f) LFG. (c); Disorganized hepatic architecture with thickened CT septa (S) forming pseudo lobules. (c & e); Dilated Hepatic sinusoids (black arrows). (d); Some hepatocytes appear swollen with pale vacuolated cytoplasm & eccentric nuclei (black arrow heads). (d & f); Nuclear changes; dark irregular nuclei are seen (asterisks), abnormal chromatin pattern (C) & margination of the nucleoli (M). (e); Cellular infiltration (Inf) in between cords of hepatocytes in e. (f); Hepatocytes with hyper eosinophilic cytoplasm & loss of granularity (yellow arrow heads) are frequently encountered. Cellular infiltration (Inf) in the portal tract area. Proliferated bile duct (D) is noticed. Cells with flattened nuclei (red arrow heads) are seen. PT; portal tract, CV; central vein, K; Kupffer cells. [H&E. (a, c & e); Mic. Mag. X 100 and (b, d & f); Mic. Mag. X400].

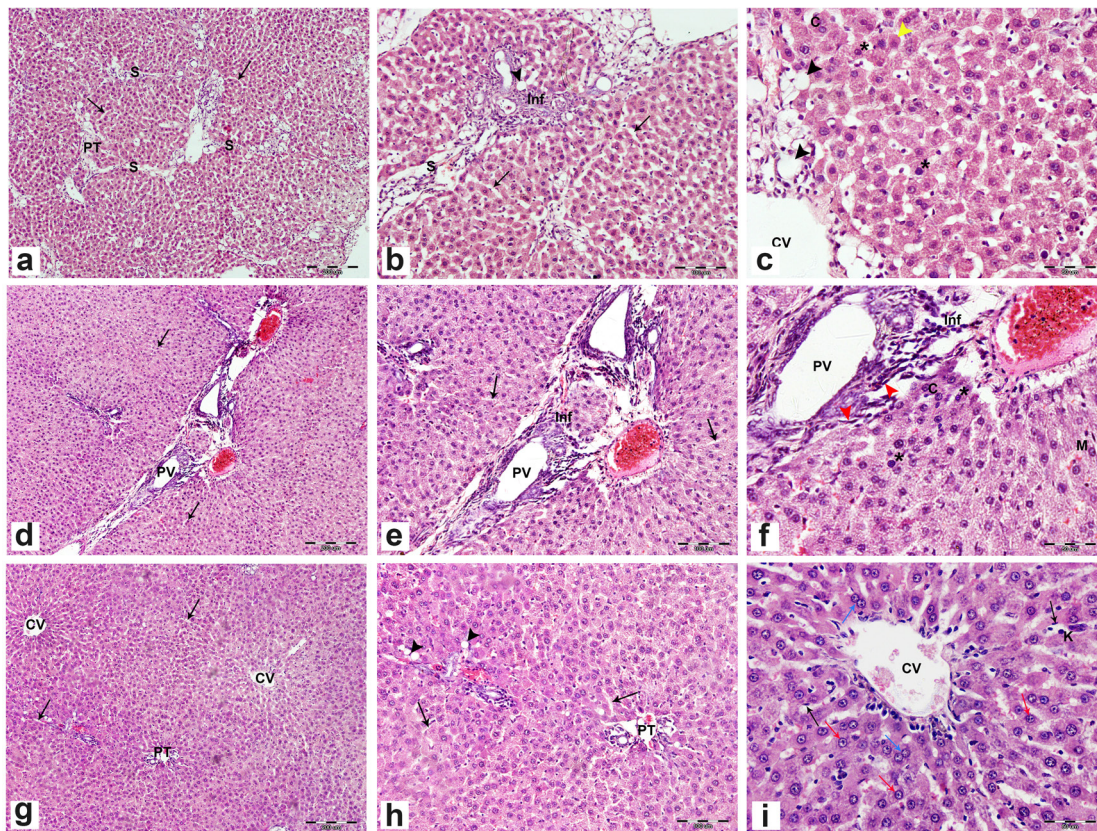


**Fig. 7:** Representative LM photographs of H & E stained liver sections (a - c) WG (a); Hepatic architecture is distorted. Thickened septa (S) connecting the PTs with the formation of pseudo lobules. (a & b); Evident widening of the hepatic sinusoids is noticed (black arrows). (b); Cellular infiltration (Inf) within the septa (S). (b & c); Some hepatocytes appear swollen (black arrow heads) with pale vacuolated cytoplasm and eccentric nuclei. (c); Other hepatocytes exhibit hyper-eosinophilic cytoplasm with loss of granularity (yellow arrow heads). Dark shrunken irregular nuclei (asterisks) and abnormal chromatin pattern (C). (d - f) BG. (d); Partially restored hepatic architecture with ill-defined arrangement of hepatocytes cords. (d & e); Limited widening of sinusoids (black arrows) is noticed. (e & f); higher magnifications of picture (d); Vascular congestion and areas with cellular infiltration (Inf) are observed in the portal area. (f); Hepatocytes still show some nuclear changes; dark shrunken irregular nuclei (asterisks), abnormal chromatin pattern (C) & margination of the nucleoli (M). Notice cellular infiltration (Inf) with flattened nuclei cells (red arrow heads) in the portal area. PV; interlobular branch of the portal vein. (g - i) BLG. (g-i); Restored hepatic architecture with no evident septa are observed. Hepatocytes appear arranged in cords radiating from the (CV) with apparent normal sinusoids (black arrows) are seen. Portal tract (PT) is well defined at the angles of the hepatic lobules. (h); Minimal vascular congestion and limited cellular infiltration in the PT. Few hepatocytes appear swollen with pale cytoplasm & eccentric nuclei (black arrow heads). (i); Most hepatocytes appear polyhedral with granular eosinophilic cytoplasm and central vesicular nuclei (red arrows). Some hepatocytes show binucleation (blue arrow). (CV); central vein, (K); Kupffer cell. [H&E, (a, d & g); Mic. Mag. X 100, (b, e & h); Mic. Mag. X 200 and (c, f & i); Mic. Mag. X 400]

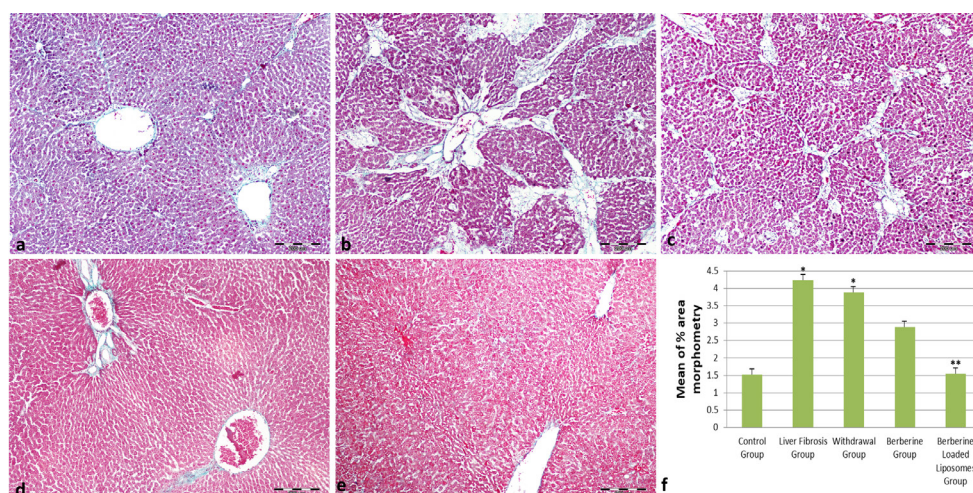


**Fig. 8:** Collagen distribution in Masson's Trichrome stained liver sections Collagen fibers are stained in green (a) CG; Minimal green trichrome stained areas surrounding the CV and PT. (b) LFG & (c) WG; Apparently increased green trichrome stained areas around the central vein, portal tracts and perisinusoidal. (d) BG; Apparently decreased green trichrome stained areas around the CV and PT. (e) BLG; minimal green trichrome stained areas around the CV and PT. [a-e; Trichrome stain, Mic. Mag. X 100] (f) Graphical representation of area % of collagen fibers. Values represent mean  $\pm$ SD (n=6). Statistical significance was determined using ANOVA test. Pairwise comparison between groups was done using Post Hoc Test (Tukey) and was considered significant when  $P \leq 0.05$ . \*Indicates significant difference compared to the CG. \*\*indicates significant difference compared to the LFG.

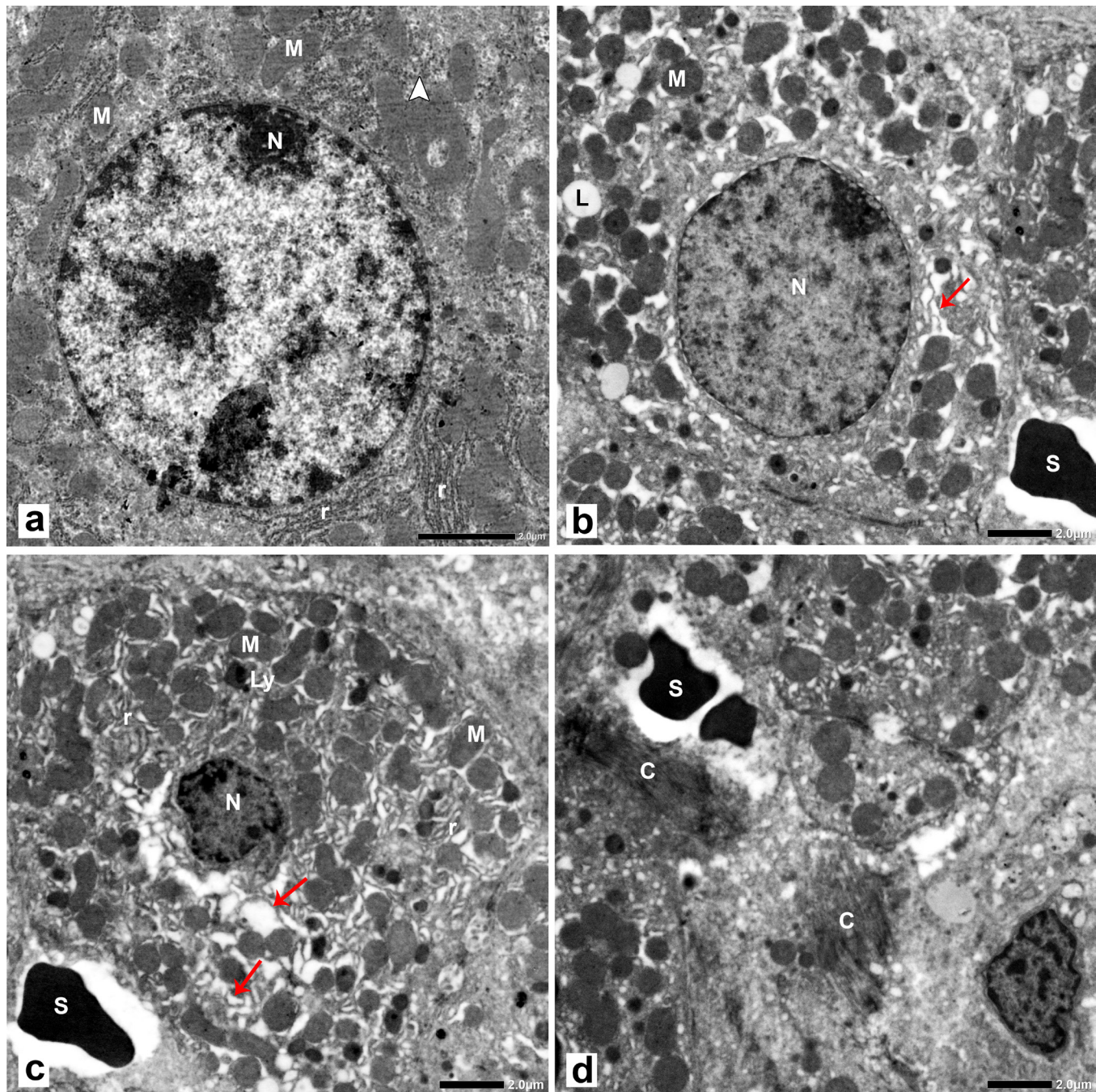


**Fig. 9:** Representative TEM micrographs of liver sections (a) CG; A hepatocyte is depicting regular euchromatic nucleus (N). Rough endoplasmic reticulum (r) appears attached to the outer nuclear membrane. Normal pattern of the mitochondria (M) is observed. Glycogen granules (arrow head) appear of normal distribution. (b-d) LFG. (b); Nucleus (N) exhibits margination of the nucleolus. (b & c); Mitochondria (M) appear deformed with indistinct cristae. Apparently dilated tubules of sER profiles (red arrow) are noticed. (L); lipid droplet. (S); blood sinusoid. (c); The nucleus (N) appears shrunken with irregular outline. Few irregular and dilated rER (r) cisternae are observed. (Ly); Lysosomes. (d); Collagen fibrils (C) deposition within the perisinusoidal space is observed. (S); blood sinusoid [TEM, Mic. Mag. a: X 3000, b-d: X 2000]

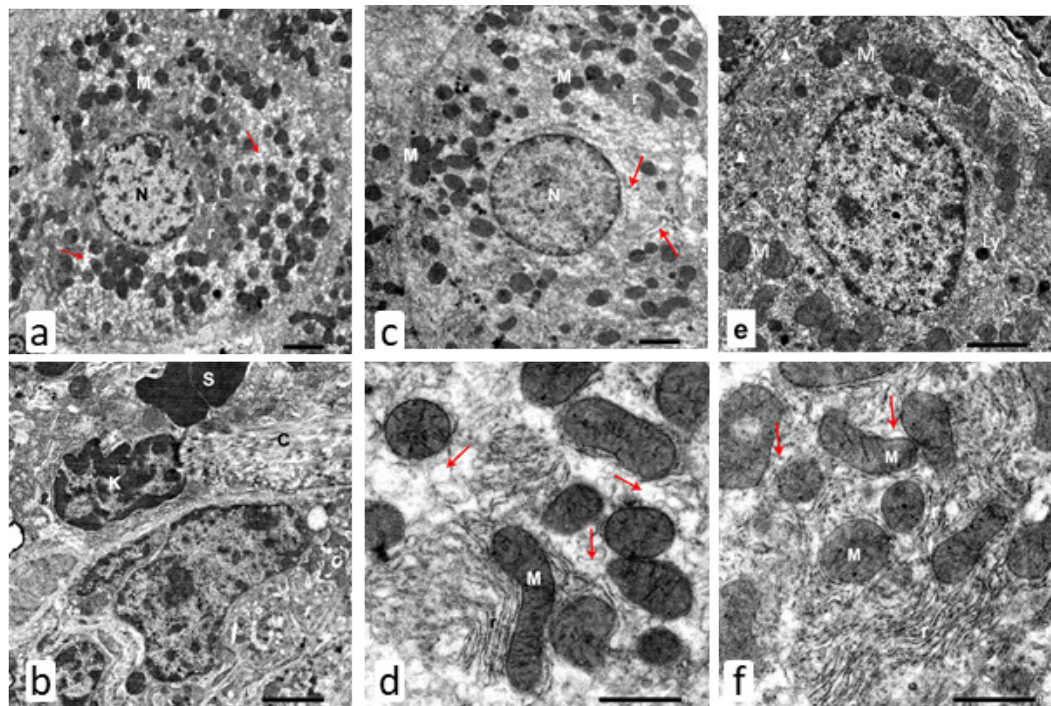


**Fig. 10:** Representative TEM micrographs of liver sections (a & b) WG. a; A hepatocyte is observed with irregular and shrunken nucleus (N). Limited profiles of rER (r) and dilated tubules of sER (red arrows) are noticed. The mitochondria (M) appear distorted with increased electron density. (b); Evident collagen fibrils (C) deposition is observed in the perisinusoidal space. (S) blood sinusoid and (K) Kupffer cell. (c & d) BG. c; A hepatocyte is seen with a rounded euchromatic nucleus (N). Few regular profiles of rER (r), and some dilated profiles of sER (red arrows) are seen. Some mitochondria (M) appear distorted with increased electron density. (d); Higher magnification of the previous photo showing distorted mitochondria (M) with some intact cristae. Few profiles of rER (r) and some dilated profiles of sER (red arrows). (e & f) BLG. e; A hepatocyte with nucleus (N) is seen with normal chromatin pattern and regular outline. Mitochondria (M) appear with regular shapes. Regular profiles of rER (r) are noticed. Abundant glycogen granules (arrow heads) and few lysosomes (Ly) are noticed. (f); Mitochondria (M) with regular shapes and restored distinct cristae. Regular profiles of rER (r) cisternae and normal pattern of the sER (red arrows) are observed. [TEM, Mic. Mag. X (a, c & e): X 2000, (b): X5000, (d & f): X 8000]

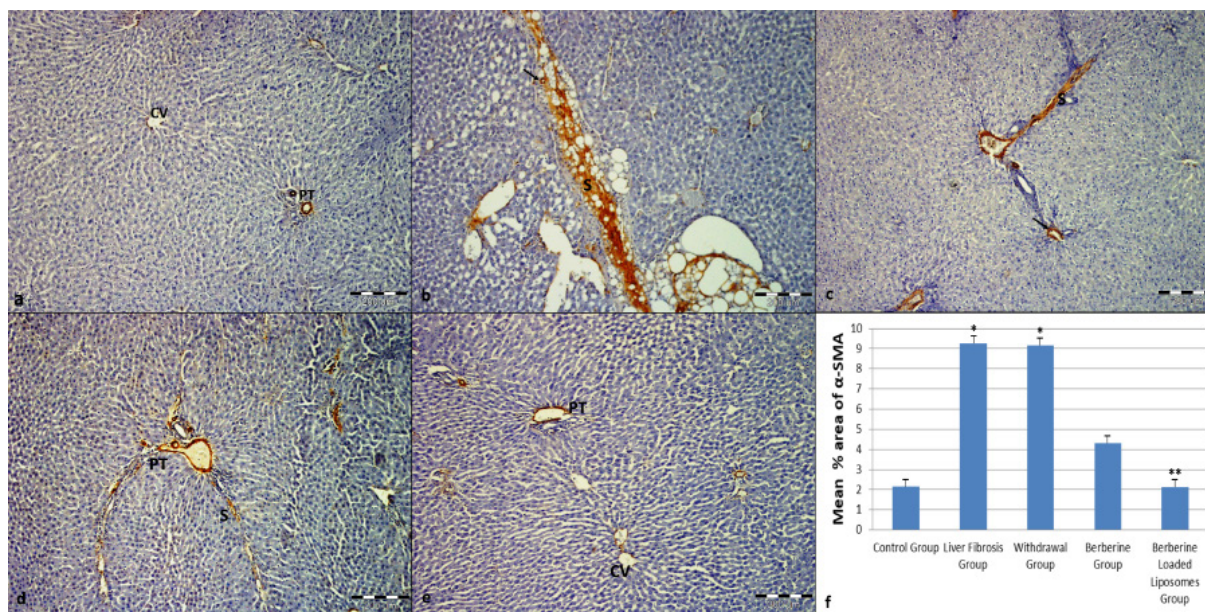


**Fig. 11:** Representative LM photographs of immunohistochemical reaction with anti  $\alpha$ -SMA in the liver tissue. (a) CG; Normal pattern of positive reaction to anti  $\alpha$ -SMA in smooth muscle cells in wall of central vein (CV) and portal tract (PT) blood vessels. (b) LFG & (c) WG ; Apparently increased  $\alpha$ -SMA immunoreactivity around portal blood vessels (arrow), extending into the connective tissue septa (S). (d) BG shows limited anti  $\alpha$ -SMA positive reaction areas in PT and septa (S). (e) BLG; shows minimal anti  $\alpha$ -SMA positive reaction areas around the CV & in PT. [a-e; Anti  $\alpha$ -SMA counterstained with hematoxylin, Mic. Mag. X100] (f) Graphical representation of area % of  $\alpha$ -SMA. Values represent mean  $\pm$ SD (n=6). Statistical significance was determined using ANOVA test. Pairwise comparison between groups was done using Post Hoc Test (Tukey) and was considered significant when  $P \leq 0.05$ . \*Indicates significant statistical difference compared to the CG. \*\*Indicates significant statistical difference compared to the LFG.

**Table 1:** Mean particle size, polydispersity index,  $\zeta$ -potential and entrapment efficiency of empty and berberine-oleate loaded liposomes

Samples	Particle size Size $\pm$ SEM <sup>a</sup> (d nm)	PDI <sup>b</sup>	ZPc $\pm$ SEM <sup>a</sup> (mV)	EE%
Empty liposomes	138.9 $\pm$ 0.43	0.345 $\pm$ 4.6	-12.6 $\pm$ 4.96	-----
BBR-OL <sup>d</sup> -loaded liposomes	192.2 $\pm$ 1.07	0.149 $\pm$ 13	-23.2 $\pm$ 3.64	78.39 $\pm$ 5.09

a n = 3

b Poly dispersity index

c zeta potential

d berberine-oleate loaded liposomes

## DISCUSSION

The liver, being a principal metabolic organ, has always attracted attention to be the core of much research work. Recently, the impact of liver diseases on human health has increased worldwide, considering the vast etiological factors that adversely affect the liver. Despite the variety of such factors, oxidative stress is implicated to be the most common underlying mechanism of hepatic injury<sup>[51,52]</sup>.

Several previous research work, has documented CCl4 to be of a hepatotoxic effect with subsequent liver fibrosis. In this regard, CCl4 induced hepatic injury in rats was the model of choice to evaluate the possible ameliorative effect of berberine oleate loaded liposomes versus berberine on CCl4 induced liver fibrosis and the associated hepatocytes degenerative changes<sup>[53]</sup>.

CCl4 is metabolized by cytochrome P450, a sER enzyme in hepatocytes, into carbon trichloride (CCl3) and (CCl3 OO) radicals. Such free radicals initiate a sequence of events within the hepatocytes, beginning by binding with macromolecules such as proteins, lipids and nucleic acids, with subsequent structural derangement of the cell membrane and subcellular organelles membrane. This is further accentuated by injurious effect of the generated reactive oxygen species (ROS), together with decreased activity of endogenous antioxidants. Eventually, a state of oxidative stress is induced where membrane phospholipids peroxidation occurs with formation of lipid peroxides. Subsequently, the permeability of the cell membranes and membranes limiting cell organelles is affected resulting in alteration of some key cellular processes. Ultimately, such a sequence of events ends up in cell necrosis. In addition, the generated free radicals induce deoxyribonucleic acids damage and afterwards cellular mutations<sup>[54,55]</sup>.

Histological assessment of the liver sections from the control subgroups demonstrated classical histological features that are encountered in a normal liver. Therefore, it was assumed that the vehicles used in the current study (distilled water and olive oil), as well as free BR and BBR-OL are considered as safe elements to the liver. Moreover, this ensured that any histological changes observed in the induced fibrosis group would be referred to the effect of CCl4.

Establishment of liver fibrosis was confirmed histologically in rats of LFG, where H & E stained liver sections revealed evident fibrotic changes, where thickened CT septa and pseudo-lobulation were seen together with distorted liver architecture and derangement of hepatocytes cords (Ishak fibrosis score 3). This was further supported by the morphometric analysis of the trichrome stained sections that revealed significantly increased collagen fibers deposition in the peri-portal area as well as in between hepatocytes, as compared to the control group.

Herein, liver fibrosis is considered as a regenerative process occurring in response to continuous or chronic exposure to injurious stimuli. Subsequently, a repair mechanism is rapidly activated to limit the damage to liver cells by producing an excessive amount of extra cellular matrix (ECM). During the early phases, hepatic injury is associated with inflammation and deposition of ECM that can be reversible if the causative agent is removed. However, in conditions of persistent or repeated injurious stimuli, hepatic regeneration is not successful, and eventually hepatocytes are replaced with an excessive amount of ECM, where the main ECM producing cell in the liver is the HSC<sup>[56]</sup>. Such fibrotic changes can be attributed to enhanced fibrogenic activity of HSCs and their trans-differentiation into myofibroblasts that express  $\alpha$ -SMA with subsequent excessive ECM deposition associated with the disruption of the ECM components and replacement by fibrillar collagen. This comes in agreement with the ultrastructural results of the present study, where collagen fibrils deposition was observed within the perisinusoidal spaces. This matrix is formed of collagen I and III and fibronectin. Such altered matrix components increase the fibrogenic effect of HSCs through production of additional matrix-bound growth factors, which eventually stimulate HSCs to migrate to the sites of tissue repair, and to start producing excessive amounts of ECM proteins<sup>[57]</sup>. In the current study, the role of HSCs and myofibroblasts was supported by the immunohistochemical results that demonstrated significant increased expression of  $\alpha$ -SMA in LFG and WG as compared to the CG, where  $\alpha$ -SMA is considered as reliable marker for myofibroblasts.

In conditions of chronic liver injury, several factors interplay to induce enhanced activity of HSCs and its transformation into myofibroblast like phenotype<sup>[56]</sup>. Initially, HSCs are stimulated by locally produced factors during the process of liver injury itself, such as lipid peroxides generated during the oxidative stress process, together with products of the damaged hepatocytes. In addition, other fibrogenic factors are produced from local cells as Kupffer and endothelial cells and induce a continuous state of HSCs hyperactivity, hence enhancing its fibrogenic potential. In this context, transforming growth factor-beta (TGF $\beta$ 1), produced from Kupffer cells is implicated in such a process. As a consequence, HSCs increase their production of several growth factors, which in turn induce their proliferation in an autocrine mode of

activation. Among such factors, is platelet derived growth factor (PDGF), which is the most potent one to induce HSCs proliferation, followed by trans differentiation into myofibroblast-like cells, that demonstrate contractile, inflammatory, and fibrogenic properties. Other autocrine factors with comparable effects include transforming growth factor  $\alpha$  (TGF $\alpha$ ) and epidermal growth factor<sup>[58]</sup>.

Increased cellular infiltration within the portal tract, as well as, in between the hepatocytes in liver sections of the fibrotic group rats was noticed. This can be referred to an inflammatory pathway, which is involved in the pathogenesis of liver fibrosis, where the immune cells are affected by activated HSCs in different ways. The net outcome is mutual interaction between HSCs and inflammatory cells, thus enhancing fibrogenesis. In such a context, Kupffer cells are influenced by the activated HSCs to produce proinflammatory cytokines such as tumor necrosis factor-  $\alpha$  (TNF- $\alpha$ ) and monocyte chemoattractant protein (MCP)-1<sup>[56]</sup>. In turn, such factors stimulate HSC's to secrete other factors such as, macrophage colony-stimulating factor (M-CSF) and interleukin 6 (IL-6) that replicate the inflammatory reaction with further activation of macrophages. Furthermore, neutrophil infiltration is stimulated by TNF- $\alpha$ <sup>[59]</sup>.

Widening of blood sinusoids was also noticed and could be secondary to portal outflow obstruction or due to inflammatory reactions in response to CCl<sub>4</sub>. Moreover, the release of mediators as vascular endothelial growth factors and IL6 might be responsible<sup>[51]</sup>. Kupffer cells appeared more prominent in comparison to control groups and were frequently encountered along the sinusoids. This comes in agreement with the fact that the Kupffer cells are one of the principal cells implicated in the pathogenesis of the liver insult considering its interaction with HSCs<sup>[51,60]</sup>.

Furthermore, liver fibrosis was associated with bile duct proliferation, where frequent cut sections of bile ducts were observed in H & E stained sections. Similar results were demonstrated by Geetha Balasubramaniam *et al*<sup>[61]</sup>. This is consistent with the release of mitogenic factors from activated HSCs as a result of the oxidative stress. As a sequence, mitotic division of the epithelial cells lining bile ductules and canals of Hering, the cholangiocytes or oval cells is triggered. The progeny of these cells may give rise to the cuboidal epithelium of the bile ducts with subsequent bile duct elongation<sup>[62,63]</sup>.

Moreover, hepatocytes depicted variable degenerative changes such as dark eosinophilic cytoplasm with loss of granularity and indistinct cellular boundaries that were more pronounced centrilobular. This comes in accordance with CCl<sub>4</sub> induced oxidative stress that is accompanied by altered membrane permeability, damage to cellular proteins and subsequently cellular necrosis<sup>[54,55]</sup>. Some other hepatocytes appeared pale and swollen with vacuolated cytoplasm and an eccentric nucleus. This histological alteration is known as vesicular steatosis, which is characterized by a single large lipid droplet that

occupies the cytoplasm of hepatocytes thus pushing the nucleus eccentrically. Such an alteration can be referred to altered lipid metabolism and inhibited lipid transport that eventually resulted in cytoplasmic accumulation of lipids within hepatocytes<sup>[64]</sup>.

In context of CCl<sub>4</sub> induced oxidative stress, different forms of nuclear changes were observed among the hepatocytes of liver fibrosis group, where some cells exhibited pyknotic nuclei, or nuclei with dissolution of chromatin. Such changes can be explained on basis of free radicals induced DNA damage<sup>[65]</sup>.

On the ultrastructural level, several changes were encountered, thus further confirming the light microscopic results. Increased dilated profiles of smooth endoplasmic reticulum were quite evident. This is attributed to enhanced activity of cytochrome P450, a sER enzyme that converts CCl<sub>4</sub> into free radical carbon trichloride (CCl<sub>3</sub>)<sup>[65,66]</sup>.

The apparent decrease in profiles of rER and glycogen granules in LFG can be interpreted on basis of free radical induced damage to cellular macromolecules and membranes<sup>[66]</sup>.

The biochemical assessment of serum albumin level was consistent with the histological results, where it showed a significant decrease in LFG compared to the CG, hence reflecting the decreased protein synthesis capacity of hepatocytes that comes in accordance with the observed decreased profiles of rER.

Moreover, mitochondria appeared distorted with indistinct cristae. Mitochondria are highly sensitive organelles to oxidative stress owing to the lipid rich nature of mitochondrial membrane, where oxidative phosphorylation is disturbed as a result of matrix protein condensation. Consequently, ATP generation and cation pump are impaired thus contributing to altered cell membrane transport, which interprets the observed cytoplasmic vacuolization in H & E stained sections of LFG. In addition, mitochondrial damage results in decreased endogenous antioxidant capacity of the cell, thus contributing to the generated oxidative stress state<sup>[67]</sup>.

The significant increase in serum levels of ALT and AST encountered in LFG as compared to the CG comes in agreement with the histological observations. ALT and AST are intracellular enzymes involved in metabolic function of the liver, thus their leakage across the cell membrane and their increased serum level reflects interrupted structural integrity of the cell membrane and altered cell membrane permeability, as well as cell degeneration.

Regarding the WG, all the histological results came almost similar to those of the fibrosis group, thus ensuring the extended toxic effect of CCl<sub>4</sub> on the liver when left unopposed with any therapeutic strategy. Furthermore, it shed some light on the limited endogenous regenerative capacity of liver, in chronic liver diseases, which ensured the necessity of adopting an effective therapeutic regimen. Biochemically, the WG did not show any significant improvement in all the assessed parameters.

Recently, “Back to Nature” is a recent worldwide attitude in pharmaceutical research, particularly in the field of nanomedicine. Natural herbal agents with anti-oxidative effect, have been of great interest in much research work. As such, in the current study, BBR was the agent of choice to assess its possible ameliorative effect on CCl<sub>4</sub> induced changes in the liver<sup>[14,15]</sup>. Nevertheless, it has been in the scope of the present study, to assess the potential enhanced therapeutic efficacy of BBR when ion-paired with oleate and loaded in liposome nanocarrier, as a novel therapeutic approach in liver fibrosis<sup>[24,25]</sup>.

Partial improvement was demonstrated in the BG that received daily IV BBR for 6 weeks. Histologically, in H & E stained sections, partial amelioration of degenerative changes and restoration of liver architecture were noticed, where pseudolobulation was less evident, but the hepatocytes were still partially disorganized (Ishak fibrosis score 2). This was further confirmed by the histomorphometric results that showed decrease in collagen deposition area percentage as compared to the LFG. Ultra-structurally, partial improvement was also noticed where some hepatocytes appeared with distinct cell boundaries and euchromatic nuclei. The biochemical results in the BG, came in accordance with the histological results. As such, ALT and AST levels were decreased, while serum albumin level increased in comparison to LFG.

Several previous attempts were adopted to use BBR in the treatment of liver fibrosis. The results of which proved the potential of BBR in ameliorating hepatic fibrosis with different mechanisms. It was found that BBR significantly down regulates the expression of  $\alpha$ -SMA, indicating that BBR might inactivate the activated HSCs. Moreover, it was postulated that the improvement of hepatic fibrosis might be partly due to the anti-oxidative activity of BBR. Moreover, a recent study demonstrated that BBR reduced mitochondrial ROS generation and thus reverses the oxidative stress<sup>[68]</sup>. In addition, BBR stimulates matrix metalloproteinase-2 (MMP-2), hence enhancing degradation of the excessively deposited matrix components. Other theories suggested that the high doses of BBR promote apoptosis of HSCs thus limiting production of excessive ECM components<sup>[14,69,70]</sup>.

In order to further enhance the effects of BBR, their use can be coupled with the use of safe and biocompatible nano-carriers. In the current investigation, liposomes were used as a delivery vehicle to ensure that the desired dose of BBR is delivered to the liver cells with minimal side effects on other body cells. It was reported that, liposomes have the ability to load a variety of drugs of different nature either lipophilic or hydrophilic. The water-soluble compounds are encapsulated into the entrapped aqueous volume of a liposome. On the other hand, drugs with lipophilic properties are incorporated into the phospholipid bilayer membrane. However, the encapsulated water-soluble molecules may suffer from a premature leakage before reaching the target organ resulted in therapeutic failure and increased potential side-effects. Therefore,

the lipophilic counterparts allow a stable incorporation into liposome membranes and taking advantages of the high loading capacity and lower the premature leakage<sup>[71]</sup>. Therefore, a BBR-OL complex was prepared using hydrophobic ion pairing approach to increase its lipophilicity and subsequently leads to high liposomal entrapment efficiency ( $78.39 \pm 5.09\%$ ). This may be due to the ability of the hydrophobic lipid bilayer compartment of liposomes to provide the region for the encapsulation of BBR-OL complex. Besides, the hydrophobic counterpart of BBR improves its membrane permeability and hence its biological activity after parenteral administration compared to the free hydrophilic BBR. In the current work, BBR-OL hydrophobic counterpart was successfully prepared and confirmed via FTIR and XRD studies.

Such enhanced effect of BBR-OL was confirmed both histologically and immunohistochemically. Histologically, remarkable restoration of the classical histological features of the liver was observed on examination of H & E stained liver sections from rats of BLG group that received BBR-OL loaded liposomes. Most of the CT septa disappeared and the general architecture was restored nearly back to normal, thus changing the state of liver fibrosis to score 1. Moreover, most of the hepatocytes depicted granular eosinophilic cytoplasm with rounded vesicular nucleus. Limited focal periportal cellular infiltration was seen. Concerning the histomorphometric results, they showed significant decrease in collagen deposition in comparison to LFG.

Immunohistochemical results came in agreement with the aforementioned results, where immune reactivity to anti  $\alpha$ -SMA in BLG revealed significantly decreased percentage area of positive reaction as compared to LFG.

This was further supported by the biochemical results, where the BLG showed a significant decrease in the liver enzymes ALT and AST, in comparison to LFG. Concerning the serum levels of albumin, significant improvement was demonstrated in comparison to LFG. This is consistent with the restored protein synthesis potential of hepatocytes and came in agreement with the ultra-structural results that showed restored regular profiles of rER.

On the ultrastructural level, marked resolution of the degenerative changes was noticed. Most of the hepatocytes appeared with distinct cell boundaries and nuclei with normal chromatin pattern. Most of the mitochondria were observed with distinct cristae and regular shapes. Regular profiles of rER were frequently encountered together with normal pattern of sER.

The present findings observed in the different TG, strongly suggest that BBR had a significant role in enhancing the regeneration of hepatocytes and the reversal of fibrosis. Furthermore, this anti-fibrotic action was synergistically enhanced by complexation with sodium oleate and loading in liposomal nanocarriers.

Regarding the liposomal drug-loading, different encapsulation techniques have been applied to encapsulate

an ion paired molecule during or after hydrophobic ion pairing. Furthermore, it was reported that, any technique that treats the formed complex as a typical hydrophobic molecule is considered valid, provided that it has not neglected the complex's sensitivity to salts and pH<sup>[49,50]</sup>. In the current work, the formed BBR-OL loaded liposomes showed promising *in-vitro* characteristics of homogenous nanometric particle size (192.2±1.07 nm) with high negative Zp magnitude (-23.2±3.64mV). Compared to the empty liposomes, the increased negative charge was suggested to be owing to the introduction of negative SO. Subsequently, more particles repulsion will occur, thus preventing their aggregation giving homogenous distribution with higher colloidal stability. These findings were further confirmed by lower PDI values of the empty liposomes as compared to the BBR-OL loaded liposomes (0.345±4.6 to 0.149±13). Furthermore, TEM micrographs of empty liposomes confirmed the formation of spherical vesicles with empty core and shell structure and nanometric size distribution. On the other hand, loaded liposomes revealed a denser core vesicle with good dispersion in water system. This proved the successful encapsulation of BBR-OL complex in the liposomes compartment.

Concerning the drug release behavior, findings could confirm the efficient incorporation of BBR-OL complex into liposomes. In addition, it acted as a reservoir system releasing BBR-OL in a sustained pattern. This may be ascribed to the time required for partitioning of the drug to aqueous medium from liposomes. Such an effect could be attributed to the involvement of drug in hydrophobic ion pair complex, which in turn increases its entrapment in the lipid bilayer of liposomes. Therefore, the postulated mechanism of BBR release involved two steps; the partitioning to release medium from liposomes and the dissolution of the released complex. Therefore, a slow release pattern was obtained which is considered beneficial for liver targeting purpose. This is important to ensure that no BBR will be leaked out of liposomes before reaching the liver after IV administration<sup>[35]</sup>. Our results demonstrated that, only 15.98±1.11% of BBR was released from BBR-OL liposomes after 30 min. Therefore, the majority of BBR would be kept inside the liposomes until it is taken up by the target organ (liver).

## CONCLUSION

This study proposed the successful development of novel integrated nanocarrier combining the benefits of both BBR-OL ion pair complex and liposomes nanocarrier. Promising *in-vitro* characteristics were developed regarding the nano-size, homogeneous distribution and the sustained release profile with minimum drug leakage. In addition, evident amelioration of fibrotic changes induced in the liver, as well as, restoration of liver structure and function, was demonstrated both histologically, immunohistochemically and biochemically. By virtue of the promising characteristics of this novel integrated nanocarrier, it was anticipated to hold promises

of enhancing the therapeutic potential of berberine on the liver fibrosis with no toxic side effects. Therefore, in such a context, its clinical use as an anti-fibrotic agent deserves further investigations.

## CONFLICTS OF INTERESTS

There are no conflicts of interest.

## REFERENCES

1. Wang F, Fan J, Zhang Z, Gao B, Wang H: The global burden of liver disease: the major impact of China. *Hepatology*. (2014); 60 (6): 2099–2108.
2. Rehm J, Samokhvalov AV, Shield KD: Global burden of alcoholic liver diseases. *J Hepatol*. (2013); 59 (1): 160–168.
3. Arsani SK, Devarbhavi H, Eaton J, Kamath PS: Burden of liver diseases in the world. *J Hepatol*. (2019); 70 (1): 151–171.
4. World Health Organization: Global Hepatitis Report Geneva: WHO. 2017.
5. Friedman SL, Bansal MB: Reversal of hepatic fibrosis - fact or fantasy? *Hepatology*. (2006); 43 (S1): S82–S88.
6. Koyama Y, Xu J, Liu X, Brenner DA: New Developments on the Treatment of Liver Fibrosis. *Dig. Dis*. (2016); 34 (5): 589–596.
7. Fallowfield JA, Iredale JP: Targeted treatments for cirrhosis. *Expert Opin Ther Targets*. (2004); 8 (5): 423–435.
8. Dienstag JL, Cosimi AB: Liver transplantation a vision realized. *N Engl J Med*. (2012); 367 (16): 1483–1485.
9. Chen S, Chen X, Lu J, Wang Y: Potent natural products and herbal medicines for treating liver fibrosis. *Chin Med*. (2015); 10 (1): 7.
10. Xianchao X, Wang H, Niu X, Liu Z, Qi Z, Wang S, Liu S: Assessment of the anti-diarrhea function of compound Chinese herbal medicine Cangpo Oral Liquid. *Afr J Tradit Complement Altern Med*. (2014); 11 (1): 140–147.
11. Meng F, Wu Z, Yin Z, Lin L, Wang R, Zhang Q: *Coptidis rhizoma* and its main bioactive components: recent advances in chemical investigation, quality evaluation and pharmacological activity. *Chin Med*. (2018); 7 (13): 13.
12. Zou K, Li Z, Zhang Y, Zhang H, Li B, Zhu W, Shi J, Jia Q, Li Y: Advances in the study of berberine and its derivatives: a focus on anti-inflammatory and anti-tumor effects in the digestive system. *Acta Pharmacol Sin*. (2017); 38 (2): 157–167.

13. Elsheikh MA, Elnaggar YS, Hamdy DA, Abdallah OY: Novel cremochylomicrons for improved oral bioavailability of the antineoplastic phytochemistry berberine chloride: Optimization and pharmacokinetics. *Int J. Phar.* (2018); 535 (1-2): 316–324.
14. Ning W, Qihe X, Hor YT, Ming H, Sha L, Man-Fung Y, and Yibin F: Berberine Inhibition of Fibrogenesis in a Rat Model of Liver Fibrosis and in Hepatic Stellate Cells. *Evid based complement Alternat Med* (2016); 2016: 1-11.
15. Tang J, Feng Y, Tsao S, Wang N, Curtain R, Wang Y: Berberine and Coptidis rhizoma as novel antineoplastic agents: a review of traditional use and biomedical investigations. *J. Ethnopharmacol.* (2009); 126 (1): 5–17.
16. Charalabidis A, Sfouni M, Bergström C, Macheras P: The Biopharmaceutics Classification System (BCS) and the Biopharmaceutics Drug Disposition Classification System (BDDCS): Beyond guidelines. *Int J Pharm.* (2019); 566: 264–281.
17. Benet LZ: The role of BCS (biopharmaceutics classification system) and BDDCS (biopharmaceutics drug disposition classification system) in drug development. *J Pharm Sci.* (2013); 102 (1): 34–42.
18. Saokham P, Muankaew C, Jansook P, Loftsson T: Solubility of Cyclodextrins and Drug/Cyclodextrin Complexes. *Molecules.* (2018); 23 (5): 1161.
19. Elnaggar YS, Elsheikh MA, Abdallah OY: Phytochylomicron as a dual nanocarrier for liver cancer targeting of luteolin: *in vitro* appraisal and pharmacodynamics. *Nanomedicine (Lond).* (2018); 13 (2): 209–232.
20. Deshmane S, Deshmane S, Shelke S, Biyani K: Enhancement of solubility and bioavailability of ambrisentan by solid dispersion using *Daucus carota* as a drug carrier: formulation, characterization, *in vitro*, and *in vivo* study. *Drug Dev Ind Pharm.* (2018); 44 (6): 1001–1011.
21. Elsheikh MA, Elnaggar YS, Gohar EY, Abdallah OY. Nanoemulsion liquid preconcentrates for raloxifene hydrochloride: optimization and *in vivo* appraisal. *Int J Nanomedicine.* (2012); 7: 3787–3802.
22. Savjani KT, Gajjar AK, Savjani JK: Drug solubility: importance and enhancement techniques. *ISRN Pharm.* (2012); 2012: 195727.
23. Sahibzada MUK, Sadiq A, Faidah HS, Khurram M, Amin MU, Haseeb A, Kakar M: Berberine nanoparticles with enhanced *in-vitro* bioavailability: characterization and antimicrobial activity. *Drug Des Devel Ther.* (2018); 12: 303–312.
24. Torkey AS, Freag MS, Nasra MMA, Abdallah OY: Novel skin penetrating berberine oleate complex capitalizing on hydrophobic ion pairing approach. *Int J. Phar.* (2018); 549 (1-2): 76–86.
25. Oliveira MS, Goulart GCA, Ferreira LAM, Carneiro G: Hydrophobic ion pairing as a strategy to improve drug encapsulation into lipid nanocarriers for the cancer treatment. *Expert Opin Drug Deliv.* (2017); 14(8): 983–995.
26. Bartneck M, Warzecha KT, Tacke F: Therapeutic targeting of liver inflammation and fibrosis by nanomedicine. *Hepatobiliary Surg Nutr.* (2014); 3 (6): 364–376.
27. LaRocque J, Bharali DJ, Mousa SA: Cancer detection and treatment: the role of nanomedicines. *Mol Biotechnol.* (2009); 42 (3): 358–366.
28. Qian W, Sun D, Zhu R, Du XL, Liu H, Wang SL: pH-sensitive strontium carbonate nanoparticles as new anticancer vehicles for controlled etoposide release. *Int. J. Nanomed.* (2012); 7: 5781–5792.
29. Peer D, Kar J, Hong S, Farokhzad OC, Margalit R, Langer R: Nanocarriers as an emerging platform for cancer therapy. *Nature.* (2007); 2 (12): 751–760.
30. Aw MS, Addai-Mensah J, Losic D: A multi-drug delivery system with sequential release using Titania nanotube arrays. *Chem Comm.* (2012); 48 (27): 3348–3350.
31. Fan M, Xu S, Xia S, Zhang X: Effect of different preparation methods on physicochemical properties of solid lipid nanoparticles. *J Agric Food Chem.* (2007); 55 (8): 3089–3095.
32. Dhiraj B, Krishnakumar S, Swaminathan S, Krishnan UM: ‘Nano-in-nano’ hybrid liposomes increase target specificity and gene silencing efficiency in breast cancer induced SCID mice. *Eur J Pharm Biopharm.* (2017); 119: 96–106.
33. Youssef SF, Elnaggar YS, Abdallah OY: Elaboration of polymersomes versus conventional liposomes for improving oral bioavailability of the anticancer flutamide. *Nanomedicine.* (2018); 13 (23): 3025–3036.
34. Freag MS, Hyaluronate-Lipid Nanohybrids: Fruitful Harmony in Cancer Targeting. *Curr Pharm Des.* (2017); 23 (35): 5283–5291.
35. Bunaciu AA, Udriștioiu EG, Aboul-Enein HY: X-ray diffraction: instrumentation and applications. *Crit Rev Anal Chem.* (2015); 45: 289–299.
36. Elsheikh MA, Elnaggar YS, Otify DY, Abdallah OY: Bioactive-Chylomicrons for Oral Lymphatic Targeting of Berberine Chloride: Novel Flow-Blockage Assay in Tissue-Based and Caco-2 Cell Line Models. *Pharm res.* (2018); 35 (1): 1–15.
37. Helvig S, Azmi IDM, Moghimi SM, Yaghmur A: Recent advances in Cryo-TEM imaging of soft lipid nanoparticles. *AIMS Biophys.* (2015); 2 (2): 116–130.

38. Scholten D, Trebicka J, Liedtke C, Weiskirchen R: The carbon tetrachloride model in mice. *Lab Anim.* (2015); 49 (1): 4–11.
39. Jones K: Intraperitoneal (IP) Injection in Rats and Mice SOP. UBC Animal Care Guidelines. (2014); 1–6.
40. Kim SO and Kim HJ. Berberine ameliorates cold and mechanical allodynia in a rat model of diabetic neuropathy. *J Med Food.* (2013);16 (6) 511–517.
41. Bishop ML, Fody EP, Schoeff LE: *Clinical Chemistry: Principles, Techniques, and Correlations.* 7<sup>th</sup> ed, Philadelphia, Lippincott Williams and Wilkins. (2013) pp 519–542.
42. Carleton HM, Drury RAB: *Carleton's Histological Technique.* 5th ed, Wallington, Description, New York, Oxford. (1980) pp 1–200.
43. Ishak K, Baptista A, Bianchi L, Callea F, De GJ, Gudat F, *et al.* Histological grading and staging of chronic hepatitis. *J Hepatol.* (1995); 22 (6): 696–699.
44. Bancroft JD, Gamble M. *Theory and Practice of Histological Techniques.* 6th ed. Philadelphia, Elsevier Health Sciences. (2008) pp 601–641.
45. Anggorowati N, Ratna Kurniasari CH, Damayanti K, Cahyanti T, Widodo I, Ghazali A, Romi M, Sari D, Arfian N: Histochemical and Immunohistochemical Study of  $\alpha$ -SMA, Collagen, and PCNA in Epithelial Ovarian Neoplasm. *Asian Pac J Cancer Prev.* (2017); 18 (3): 667–671.
46. Schindelin J, Rueden CT, Hiner MC, Eliceiri KW: The Image J ecosystem: an open platform for biomedical image analysis, *Mol. Reprod. Dev.* (2015); 82 (7-8): 518–529.
47. Ord JK. *Encyclopedia of Statistical Sciences,* John Wiley and Sons. (2004) pp 12.
48. Jaafar-Maalej C, Diab R, Andrieu V, Fessi H: Ethanol injection method for hydrophilic and lipophilic drug-loaded liposome preparation. *J. Liposome Res.* (2010); 20 (3): 228–243.
49. Elsheikh MA, Elnaggar YS, Gohar EY, Abdallah OY: Nanoemulsion liquid preconcentrates for raloxifene hydrochloride: optimization and *in vivo* appraisal. *Int J Nanomed.* (2012); 7: 3787–3802.
50. Kurt D, Robert K: Hydrophobic ion pairing: encapsulating small molecules, peptides, and proteins into nanocarriers. *Nanoscale Adv.* (2019); 1: 4207–4237.
51. Mao G, Kraus GA, Kim I, Spurlock ME, Bailey TB, Beitz DC: Effect of a mitochondria-targeted vitamin E derivative on mitochondrial alteration and systemic oxidative stress in mice, *Br J Nutr.* (2011); 106 (1): 87–95.
52. Cesaratto L, Vascotto C, Calligaris S, Tell G: The importance of redox state in liver damage, *Ann Hepatol.* (2004); 3 (3): 86–92.
53. Igoniya P, Singh CS, Shukla A: A comprehensive review of different liver toxicants used in experimental pharmacology. *Int J Pharm Sci Drug Res.* (2009); 1 (3): 124–135.
54. Boll, Meinrad, Lutz, W. D., Becker, Eberhard and Stampfl, Andreas. Mechanism of Carbon Tetrachloride-Induced Hepatotoxicity. *Hepatocellular Damage by Reactive Carbon Tetrachloride Metabolites. Zeitschrift für Naturforschung C.* (2001); 56 (7-8): 649–659.
55. Al-Rasheed NM, Fadda LM, Ali HM, Abdel Baky NA, El-Orabi NF, Yacoub HI: New mechanism in the modulation of carbon tetrachloride hepatotoxicity in rats using different natural antioxidants. *Toxicol. Mech. Methods.* (2016); 26: 243–250.
56. Roehlen N, Crouchet E, Baumert TF: Liver Fibrosis: Mechanistic Concepts and Therapeutic Perspectives. *Cells.* (2020); 9 (4): 875.
57. Chen W, Rock JB, Yearsley MM, Ferrell LD, Frankel WL: Different collagen types show distinct rates of increase from early to late stages of hepatitis C-related liver fibrosis, *Hum Pathol.* (2014); 45: 160–165.
58. Higashi T, Friedman SL, Hoshida Y: Hepatic stellate cells as key target in liver fibrosis. *Adv Drug Deliv Rev.* (2017); 121:27–42.
59. Parsons CJ, Takashima M, Rippe RA: Molecular mechanisms of hepatic fibrogenesis., *J Gastroenterol Hepatol.* (2007); 22: S79–84.
60. Yousefi-Manesh H, Shirooie S, Partoazar A, Nikoui V, Estakhri MRA, Bakhtiarian A: Hepatoprotective effects of phosphatidylserine liposomes on carbon tetrachloride-induced hepatotoxicity in rats. *J Cell Biochem.* (2019); 120: 11853–11858.
61. Balasubramaniam G, Sekar M, Varadarajan M, Badami S. Antioxidant and Hepatoprotective Activities of *Strobilanthes kunthianus* against Carbon Tetrachloride-Induced Hepatotoxicity in Rats. *Pharmacog. Journ.* (2020); 12 (5): 1143–1151.
62. Sato K, Marzioni M, Meng F, Francis H, Glaser S, Alpini G: Ductular reaction in liver diseases: pathological mechanisms and translational significances. *Hepatol.* (2019); 69 (1): 420–430.
63. Kumar V, Abbas AK, Aster JC. *Robbins basic pathology,* Philadelphia, Saunders, 2012, pp 1–30.
64. Tandra S, Yeh MM, Brunt EM, Vuppalanchi R, Cummings OW, Unalp-Arida A, Wilson LA, Chalasani N: Presence and Significance of Microvesicular Steatosis in Nonalcoholic Fatty Liver Disease. *J Hepatol.* (2011); 55 (3): 654–659.
65. Muriel P: Role of free radicals in liver diseases. *Hepatol Int.* (2009); 3 (4): 526–536.

66. Maiers JL, Malhi H: Endoplasmic Reticulum Stress in Metabolic Liver Diseases and Hepatic Fibrosis. *Semin Liver Dis.* (2019); 39 (2): 235–248.
67. Mansouri A, Gattolliat CH, Asselah T: Mitochondrial Dysfunction and Signaling in Chronic Liver Diseases. *Gastroenterology.* (2018); 155 (3): 629–647.
68. Sun, Y., Yuan, X., Zhang, F. *et al*: Berberine ameliorates fatty acid-induced oxidative stress in human hepatoma cells. *Sci Rep.* (2017); 7: 11340.
69. Feng, Siu KY, Ye X, Wang N, Yuen MF, Leung CH, Tong Y, Kobayashi S: Hepatoprotective effects of berberine on carbon tetrachloride-induced acute hepatotoxicity in rats. *Chin Med.* (2010); 5: 33.
70. Naim A, Pan Q, Baig MS: Matrix metalloproteinases (MMPs) in liver diseases. *J Clin Exp Hepatol.* (2017); 7: 367–372.
71. Khalifa AM, Elsheikh MA, Elnaggar YSR: Current strategies for different paclitaxel-loaded Nano-delivery Systems towards therapeutic applications for ovarian carcinoma: A review article. *J Control Release.* (2019); 311–312: 125–137.

## الملخص العربي

# الجسيمات الشحمية المتكاملة المحملة بالبربارين لإدارة تليف الكبد المستحث تجريبياً في الجرذان: دراسة هستولوجية وهستوكيميائية مناعية

ولاء عبد السلام أحمد عمر<sup>١</sup>، ناهد إبراهيم زهدى<sup>١</sup>، ثناء حسن صبرى راضى<sup>١</sup>، منال عبد الواحد حسن الشيخ<sup>٢</sup>، رحاب أحمد عبد المنعم<sup>١</sup>

<sup>١</sup>قسم الهستولوجيا وبيولوجيا الخلية، كلية الطب، جامعة الإسكندرية

<sup>٢</sup>قسم الصيدلانيات، كلية الصيدلة، جامعة دمنهور

**المقدمة:** يعتبر تليف الكبد جزءاً لا يتجزأ من مسارات معظم أمراض الكبد المزمنة. إنها عملية ديناميكية تتميز بإصابة الكبد المزمنة المصحوبة بتراكم الكولاجين. في الآونة الأخيرة، اكتسب نهج "العودة إلى الطبيعة" واستخدام العلاجات العشبية اهتماماً كبيراً في جميع أنحاء العالم البربارين هو أحد الأدوية العشبية التي تمتلك مجموعة متنوعة من التأثيرات الدوائية بما في ذلك التأثيرات الوقائية للكبد، والمضادة للالتهابات و للتليف. ومع ذلك، فهي تعاني من نفاذية غشائية محدودة بسبب طبيعتها المحبة للماء. في نطاق هذا السياق، استهدفت الدراسة الحالية إنتاج مركب أيوني كاره للماء من أوليات البربارين مدمج مع الجسيمات الشحمية المتناهية الصغر و دراسة الفعالية العلاجية كوسيلة لتحسين تليف الكبد المستحدث بواسطة رابع كلوريد الكربون في ذكور الجرذان البيضاء البالغة.

**مواد وطرق البحث:** تم تحضير مركب البربارين وتحميله في الجسيمات الشحمية متبوعاً بالتوصيف الفيزيوكيميائي في المختبر. ثم تم دراسة تأثيره العلاجي في نموذج التليف الكبدي في الجرذان مقارنة مع البربارين الحر بواسطة التقييم الكيميائي الحيوي و الهستولوجي والهستوكيميائي المناعي لعينات الدم و الكبد.

**النتائج:** أظهرت الجسيمات الشحمية المتناهية الصغر المتكاملة المقترحة حجم نانومتري ( $192,2 \pm 1,07$  نانومتر) ونمط إطلاق مستدام مع الحد الأدنى من تسرب الدواء. أظهرت الجرذان التي تلقت البربارين المحمل في الجسيمات الشحمية المتناهية الصغر تحسناً واضحاً في التغيرات التنكسية وترسب ألياف الكولاجين من تلك التي تلقت البربارين منفرداً.

**الاستنتاج:** تم تطوير تجميع نانوي جديد ومتكامل من الجسيمات الشحمية المحملة بالبربارين بنجاح كأداة واعدة لعلاج فعال لتليف الكبد فالتقنيات المطبقة للتقييم الهستولوجي والهستوكيميائي الحيوي قد أثبتت كفاءة البربارين المحمل علي الجسيمات الشحمية متناهية الصغر في استعادة البنية التركيبية لخلايا الكبد والوظائف الكبدية.